SCIENCE CHINA
Life Sciences

•RESEARCH PAPER•

February 2020 Vol.63 No.2: 290–300
https://doi.org/10.1007/s11427-018-9559-x

Decreasing intraocular pressure significantly improves retinal vessel density, cytoarchitecture and visual function in rodent oxygen induced retinopathy

Rui Du[1], Xu Wang[1], Ke Shen[1] & Shigang He[1,2,3*]

[1]*School of Biomedical Engineering, Shanghai Jiao Tong University, Shanghai 200240, China;*
[2]*Institute of Natural Sciences, Shanghai Jiao Tong University, Shanghai 200240, China;*
[3]*Bio-X Institute, Shanghai Jiao Tong University, Shanghai 200240, China*

Received June 25, 2019; accepted August 8, 2019; published online November 12, 2019

We attempted to explore a noninvasive, easily applicable and economically affordable therapy for retinopathy of prematurity (ROP). Rat pups were raised in 80% oxygen from postnatal day 7 to P12, and returned to room air. Travoprost eye drops were administered twice a day for 7 days, to reduce intraocular pressure (IOP) by about 20%. Immunohistochemical staining was performed to visualize vessel endothelial cells, to analyze retinal neurons and cytoarchitecture. Behavioral experiments were carried out to test visual acuity and contrast sensitivity. At the end of the 7-day treatment, the number of vessels extending to the vitreous body was significantly reduced and retinal vessel density increased. This improvement was maintained to the end of the 12th week. In the central retina of the model group, the horizontal cells were completely wiped out, the outer plexiform layer was undetectable, and the rod bipolar cell dendrites sprouted into the outer nuclear layer. The treatment partially reverted these architectural changes. Most importantly, behavioral experiments revealed significantly improved visual acuity and contrast sensitivity in the treated group. Therefore, reducing IOP could potentially serve as a safe and economical measure to treat ROP.

oxygen induced retinopathy, vessel plasticity, visual acuity, contrast sensitivity, rat

Citation: Du, R., Wang, X., Shen, K., and He, S. (2020). Decreasing intraocular pressure significantly improves retinal vessel density, cytoarchitecture and visual function in rodent oxygen induced retinopathy. Sci China Life Sci 63, 290–300. https://doi.org/10.1007/s11427-018-9559-x

INTRODUCTION

Retinopathy of prematurity is a disease with a clear etiology (Campbell, 1951; Patz et al., 1952). There are three phases: induction, progression and recession.

In the induction phase, high concentration oxygen abolishes physiological hypoxia, deters retinal vessel development and even induces vessel degeneration (Ashton et al., 1953; Patz, 1954). This results in a large avascular peripheral area in humans (Smith, 2003) and in rodents a retina with very low vascular density especially in the central area (Patz et al., 1953; Smith et al., 1994).

In the progression phase, room air becomes hypoxic due to severely retarded vasculature, which results in the formation of neovascular tufts, the tortuosity of vessels and a massive abnormal proliferation of vessels, many of which extend into the vitreous body (Friedenwald et al., 1951; Ashton, 1954; Patz, 1982). This is the most critical phase because the abnormal vessels extending into the vitreous may form filaments and cause retinal detachment and eventually blindness (Krause, 1946).

In the recession phase, most retinal abnormalities spontaneously recess, except for the tortuosity of vessels. The retinal vasculature appears quite normal. This happens in moderate and mild human ROP (O'Connor et al., 2004; Moskowitz et al., 2005; Goldenberg et al., 2008; Lorenz et

*Corresponding author (email: shiganghe@sjtu.edu.cn)

© Science China Press and Springer-Verlag GmbH Germany, part of Springer Nature 2019

al., 2009) and all rodent OIR (Penn et al., 1993; Connor et al., 2009; Lange et al., 2009). However, careful quantification in the rat retina still revealed long lasting reduction in vessel density and impaired visual function (Wang et al., 2019). This finding may elucidate the mechanism for functional deficits in moderate or mild human ROP.

Currently, most interventions take place in the late stage of the progression phase as retrospective and corrective measures. One commonly performed treatment is to ablate the avascular peripheral retina using photocoagulation (McNamara et al., 1991; Early Treatment for Retinopathy of Prematurity Cooperative Group, 2003) or cryotherapy (Elsas et al., 1988; Elsas et al., 2001), therefore to quench the induction signal for vessel proliferation. This leads to permanent impairment of peripheral vision. The other is to use anti VEGF antibodies to suppress vessel growth (Chung et al., 2007; Shah et al., 2007; Mintz-Hittner et al., 2011; Stahl et al., 2018). This is also potentially problematic since the retina is hypoxic and needs vessel innervation to provide oxygen and nutrients necessary for retinal development and function. Suppressing vessel growth in this early postnatal stage may impair the development of retinal neurocircuitry and visual functions (Asano and Dray, 2014).

Ricci and colleagues (Ricci et al., 1991) pioneered a more creative and preventative method: to reduce the intraocular pressure (IOP). Apparently, reducing IOP during the proliferation stage increases perfusion efficacy, relieves the hypoxic condition, and therefore reduces abnormal vessel proliferation. One thing not very clear to us is that they started the treatment as soon as the pups entered the oxygen chamber. During the hyperoxic period, reducing the IOP could increase perfusion efficacy (Xin et al., 2018) and may promote vessel degeneration, causing detrimental consequences to the animals.

In this study, we modified Ricci's protocol, used clinically available medicine to reduce the IOP as soon as the pups leave the oxygen chamber, i.e., when the retina became hypoxic. We evaluated the retinal vessel density, retinal cytoarchitecture and visual function to assess the effectiveness of this intervention, hoping to provide a non-invasive and preventative therapy to the ROP.

RESULTS

Interval and mechanism of treatment

We continuously monitored the intraocular pressure (IOP) of both eyes when administered the eye drop in one eye. It is apparent that the IOP of both eyes started to decrease after 2 h, reaching the lowest at about 10 h, and recovered at around 24 h (Figure S1A in Supporting Information). Therefore, we chose to administer the eye drops to both eyes at an interval of 12 h to maintain the IOP continuously at a low level.

To exclude side effects other than the decrease of IOP, we also reduced the IOP physically by puncturing the sclera. In this case, the IOP dropped immediately after the puncture, and started to recover in 4 h (Figure S1B in Supporting Information). We performed a puncture every 4 h over a 12 h period each day for 7 days to keep the IOP at a low level for a comparable duration to the eye drop treatment.

Alleviation of vascular abnormalities

As we reported in a previous paper, in the animals raised in 80% oxygen, the number of vessels extending into vitreous body increased and the retinal vessel density decreased (Wang et al., 2019). At the end of the 7-day treatment, the number of vessels extending into the vitreous body was significantly reduced (38.9%±4.3%), and the retinal vessel density significantly increased (superficial: 21.7%±4.6%, deep: 38.4%±11.7%). The group in which the IOP was reduced physically showed a larger reduction in abnormal vessel intrusion (34.9%±2.9%) and a larger increase in retinal vessel density (superficial: 41.0%±5.5%, deep: 41.0% ±10.8%) (Figure 1). These results indicated that the improvements resulted from decreased IOP.

We followed up the retinal vessel density to the age of the 8 and 12 weeks. The vessel density of the superficial layer was reduced in the OIR groups (Figure 2B and G) and was partially recovered in the treated retinas (Figure 2C and G). The vessel density in the deep layer exhibited a similar but more significant change than that in the superficial layer (Figure 2E, F and H). These results showed that the improvements observed at the end of treatment could be maintained over an extended period of time.

The restoration of changing retinal cytoarchitecture

We examined the cytoarchitectural changes of the retina at two time points, postnatal week 8 and 12. There is no difference in any parameter measured between these two time points; therefore, only data collected at 8 weeks are presented in the following section.

First, we measured the thickness of different sublamina in DAPI stained cross sections of control (Figure 3A), OIR (Figure 3B) and treatment groups (Figure 3C). The magnified section indicated the sublaminae (Figure 3D). There was no difference in the thickness of the outer nuclear layer (ONL) (Figure 3E and F). The outer plexiform layer (OPL) was immeasurable in the OIR retinas except the far periphery (arrowhead in Figure 3B), whereas in the treated retinas, the immeasurable OPL was only in the most central region (arrowheads in Figure 3C). In the peripheral retina, there is no

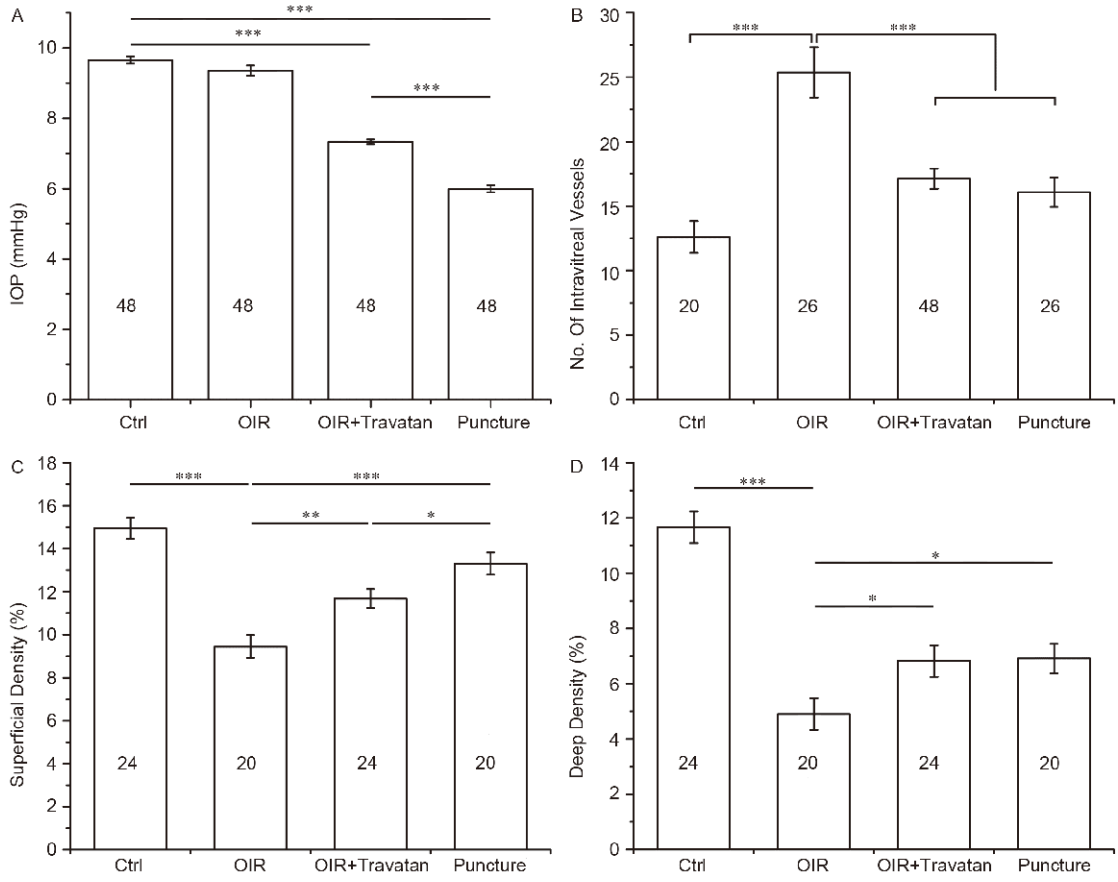

Figure 1 IOP was measured during the treatment and the vessel abnormalities at P20. A, IOP measurements of OIR, Puncture and OIR+Travatan eyes for 7 days, once daily. B, The number of vessels extending into the vitreous body was counted in Control, OIR, Puncture and OIR+Travatan groups at P20. The retinal vessel density of Control, OIR, Puncture and OIR+Travatan groups in the superficial (C) and deep (D) layers. Animal numbers are shown in each column. *, $P<0.05$; **, $P<0.01$; ***, $P<0.001$.

difference in thickness of the OPL between three groups (Figure 3F). The INL and the IPL were thinner in the OIR group and no apparent recovery was observed in the treatment group (Figure 3E and F). The thickness of the GCL was not affected (Figure 3E and F).

We also measured the length of the section where the OPL was immeasurable. There was a large section immeasurable OPL in the OIR group and the treatment significantly reduced this section (Figure S2 in Supporting Information).

Next, we quantified various retinal neurons in the preparations stained with various cell type specific antibodies.

Horizontal cells

We used calbindin to stain horizontal cells. In the OIR retinas, horizontal cells completely disappeared in the central retina, corresponding to the region where the OPL was absent (Figure 4B and D). In the treated group, the region lacking the OPL was reduced and so was the region lacking horizontal cells (Figure 4C and D). The density of horizontal cells in the peripheral retina was similar in different groups (Figure 4D).

Rod bipolar cells

We used PKCα to stain rod bipolar cells. The density of rod bipolar cells was reduced in the central retina in the OIR group (Figure 5B and E), and their dendrites sprouted into the ONL (Figure 5D and F). In the treated group, the reduction in the density of rod bipolar cells was alleviated, and the sprouting of dendrites suppressed (Figure 5E and F). In the peripheral retina, both the density and morphology of rod bipolar cells were quite normal in all groups (Figure 5E and F).

Calretinin amacrine cells

We stained the retina with an antibody against calretinin. This antibody clearly stained the cholinergic amacrine cells in the INL and displaced cholinergic amacrine cells in the GCL in addition to some other amacrine cells stratifying in the middle of two cholinergic bands (Figure 6A). The density of the cells in the INL was significantly lower in the central and peripheral retina in the OIR and the treated groups (Figure 6B and D), whereas no significant difference in density was observed in the GCL among three groups (Fig-

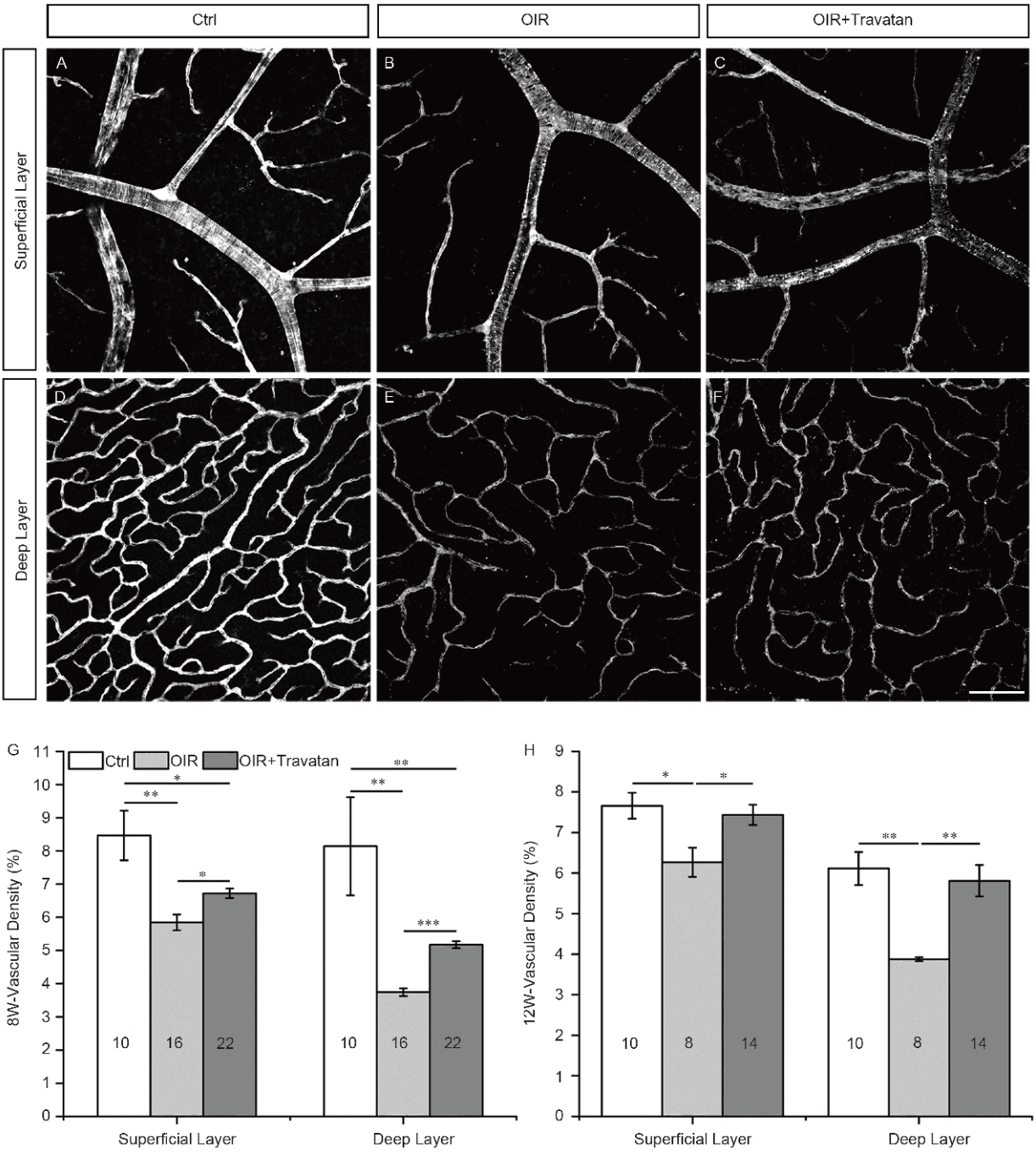

Figure 2 Retinal vessels in 8-week-old and 12-week-old control, OIR and OIR+Travatan rats. Magnification images of retinal vessels of control, OIR and Travatan groups at 8-week-old in superficial (A, B, C) and deep (D, E, F) layers, respectively. Summary of retinal vessel density in control, OIR and OIR +Travatan animals in superficial and deep layers at 8-week-old (G) and 12-week-old (H). The number of rats quantified is shown in each column. *, $P<0.05$; **, $P<0.01$; ***, $P<0.001$. Scale bar, 100 μm.

ure 6B and E). The width spanning three calretinin positive bands (a) remained constant in all three groups (Figure 6B, C and F). However, the distance between the innermost calretinin band (b) and the GCL was significantly reduced both in the central and peripheral retina in the OIR group and remained reduced in the treated group (Figure 6B, C and G). This reduction almost completely accounted for the reduction in thickness of the IPL (Figure 2).

The improvement of visual function

To us, the most important improvement is the improvement of visual function. We utilized a behavioral paradigm to test visual acuity and contrast sensitivity (Prusky et al., 2000; McGill et al., 2004; Ren et al., 2012; Wang et al., 2019). The OIR caused the threshold spatial frequency to decrease and threshold contrast to increase (Figure 7A and B). It is clear

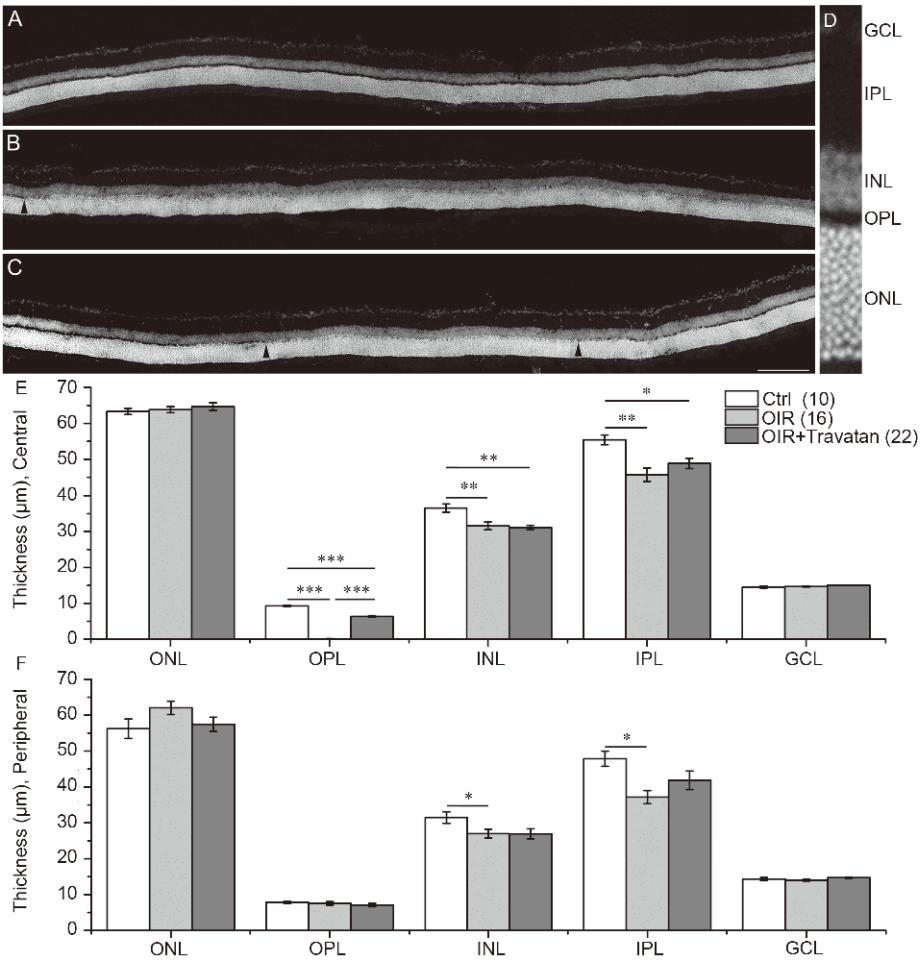

Figure 3 The thickness of different sublaminae cross sections of control, OIR and OIR+Travatan groups. The retinal cross section of control (A), OIR (B) and OIR+Travatan (C) stained by DAPI. Black arrowheads pointed to the terminal of OPL wiped out area in panel B and C. The retina sublamiane was indicated on magnified section (D). The thickness measurement of central (E) and superficial (F) retinal sublaminae cross sections of control, OIR and OIR +Travatan groups. The number of rats is shown in the legends. *, P<0.05; **, P<0.01; ***, P<0.001. Scale bar, 200 μm.

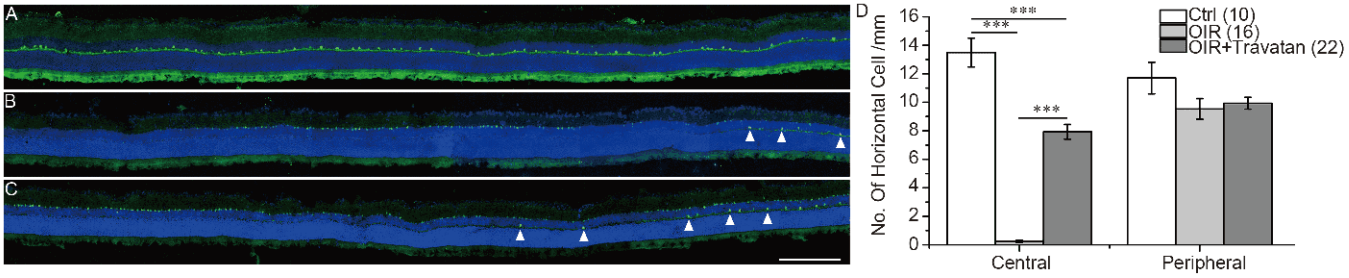

Figure 4 Lower IOP protected the horizontal cell loss. The horizontal cell was stained with calbindin (green) of control (A), OIR (B) and OIR+Travatan (C) groups. The white arrowhead pointed to the horizontal cell soma in panel A and B. Travatan rescued the density decrease of horizontal cells in the central retina (D). The number of rats is shown in the legends. ***, P<0.001. Scale bar, 250 μm.

that the threshold spatial frequency increased, although still lower than the control (Figure 7A), and threshold contrast decreased to a level comparable to the control in the treated group (Figure 7B). The improvement was maintained to the 12th week (Figure 7A and B), suggesting long-lasting therapeutic effects. The tendency of visual function is shown in Figure S3 in Supporting Information.

DISCUSSION

Treating ROP by reducing IOP

As mentioned in the Introduction, we reason that starting reducing IOP when the retina was under hyperoxic condition would enhance perfusion efficiency and exacerbate vessel degeneration (Ricci). However, Ricci and colleagues did find

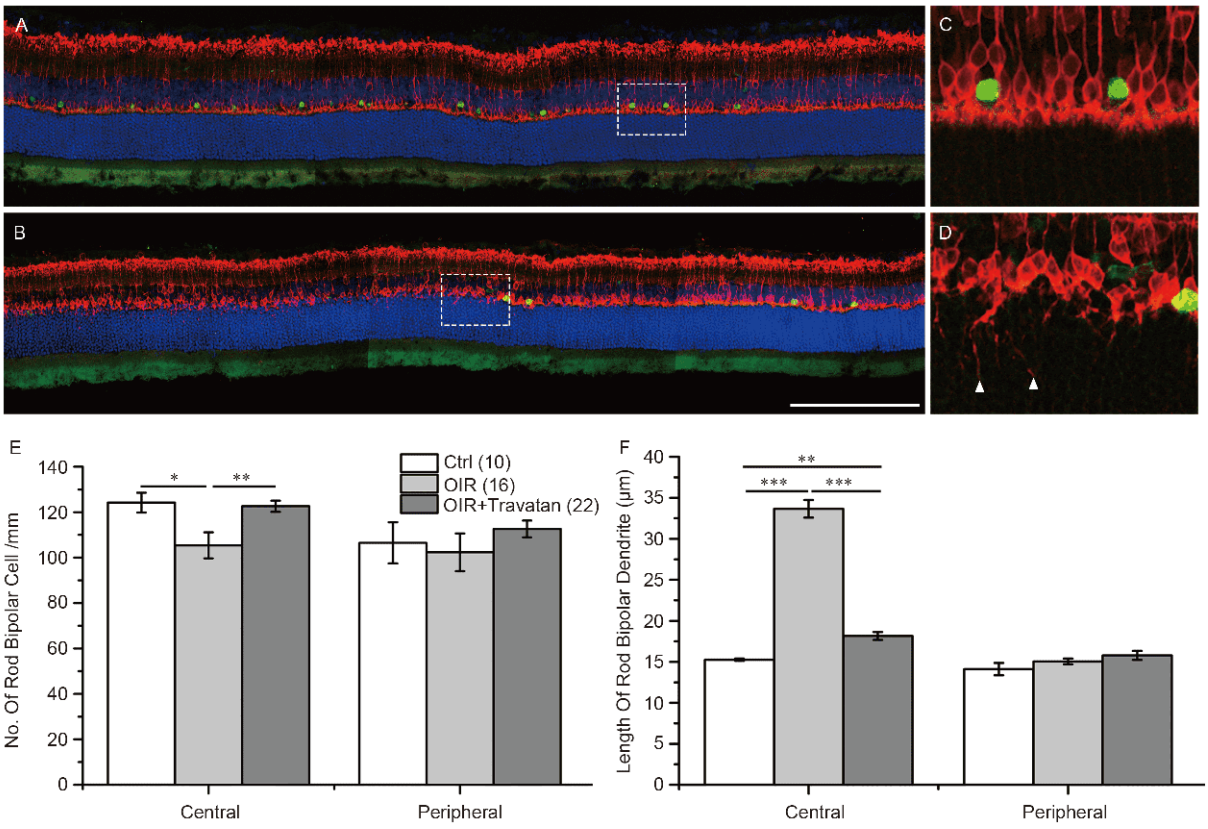

Figure 5 The abnormalities of rod bipolar cells. Rod bipolar cells (red) were stained with PKCα in the control (A) and OIR (B) retinal cross section. C and D show magnification area marked by the rectangle in A and B. White arrowheads pointed to the dendrites sprouting. The summary density and length of rod bipolar cells of three groups are shown in E and F, respectively. The number of animals is shown in the legends. *, $P<0.05$; **, $P<0.01$; ***, $P<0.001$. Scale bar, 200 μm.

the treatment still effective in reducing neovascularization and hemorrhagic lesions after the pups returned to the normal air (Ricci et al., 1991).

Our previous study provided a potential explanation. We found that there is a minimal level of vessel innervation, irrespective of exposing more immature retina by advancing initiation and lengthening exposure duration (Wang et al., 2019). When the high concentration of oxygen already suppressed the retinal vasculature to the minimal level, an increase in perfusion efficiency due to decreased IOP was unlikely to cause any further vessel loss, therefore further functional deterioration.

In this study, we modified Ricci and colleagues' protocol, started the treatment when the pups left the oxygen chamber and when the retina became hypoxic. We evaluated the therapeutic effects by examining retinal vessel density, retinal cytoarchitecture and performance of visually guided behavior. We found that maintaining the IOP about 20% lower than the normal level for a week significantly increased retinal vessel density, restored retinal architecture and rescued visual function. Two points need to be mentioned. First, in this experiment we used 0.9% saline as a control, rather than the exact vehicle of the medicine. Second, the control of physically reducing the IOP induced some damage to the sclera and some stress to the animals. These procedures may confound the conclusions we hope to achieve.

Implications of the retinal cytoarchitecture

A few alterations in retinal cytoarchitecture may underlie functional consequences (Zhang et al., 2018; Liu et al., 2019; Qiao et al., 2019; Zhang et al., 2019). The most striking change is the disappearance of the OPL. Normally in the OPL, the photoreceptor terminals contact bipolar cell dendrites, and the horizontal cell processes mediate lateral interactions.

A few factors accounted for this dramatic change. First and foremost, horizontal cells completely disappeared in the central retina. In the rodent retina, all horizontal cells are axon bearing type B cells (Suzuki and Pinto, 1986; Peichl and Gonzalez-Soriano, 1993). The dendrites of the horizontal cells feedback to cone pedicles (Kolb, 1974) and axon terminals feedback to rod spherules (Sandman et al., 1996). Loss of horizontal cells accounted for the loss of a major component of the OPL. It appeared that the hypoxia hit

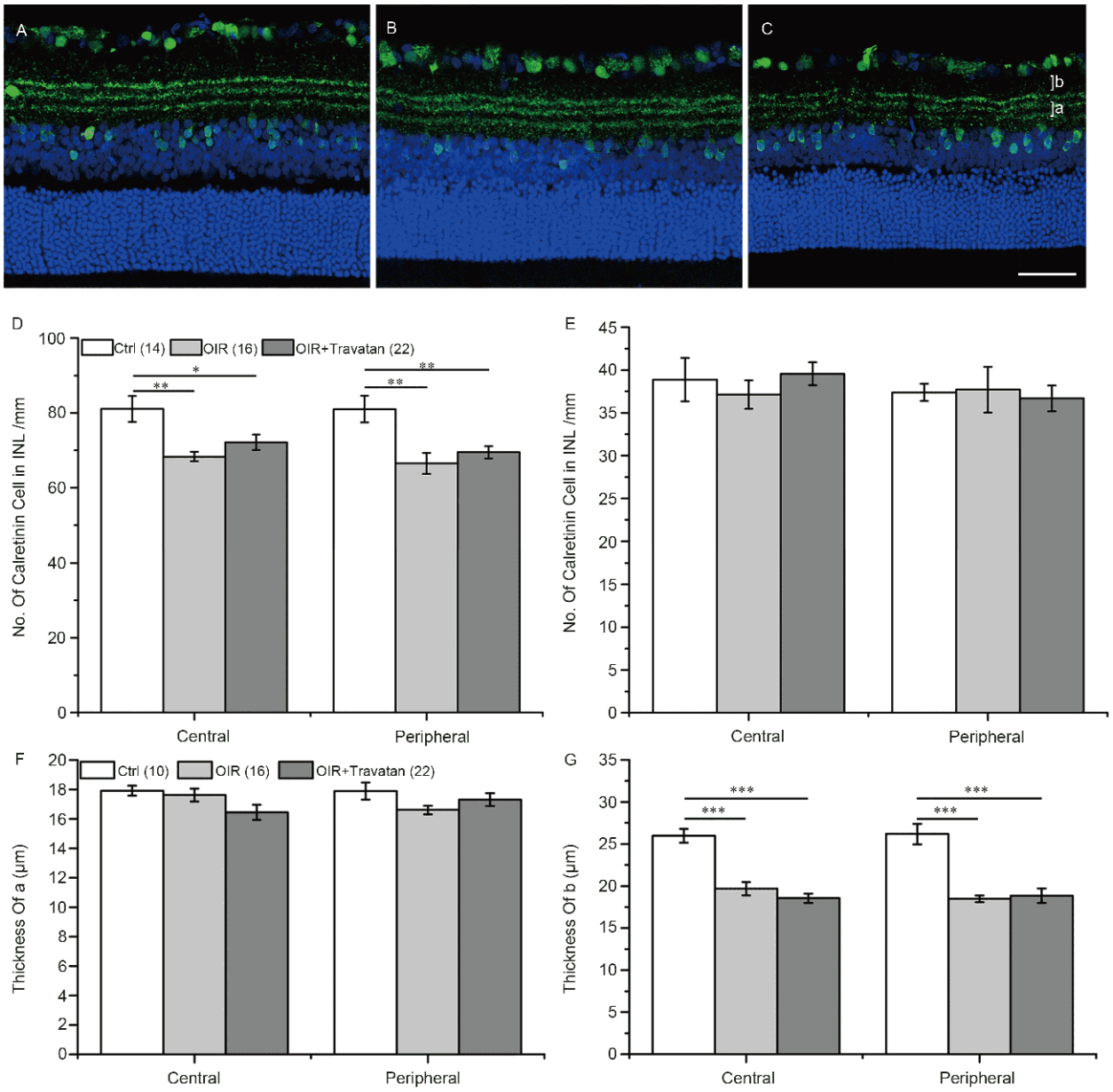

Figure 6 Hyperoxia led to the abnormalities of calretinin-containing amacrine cells. The cholinergic amacrine cells (green) were stained with calretinin antibody in the retinal cross sections of control (A), OIR (B) and OIR+Travatan (C) groups. The summary density of calretinin amacrine cells in INL (D) and GCL (E). The summary thickness of a (F) and b (G). The number of rats is shown in the legends. *, $P<0.05$; **, $P<0.01$; ***, $P<0.001$. Scale bar, 50 μm.

the horizontal cells particularly hard, probably because the long axons and large terminals are highly demanding for energy supply.

Second, the rod bipolar cells exhibited two alterations in the central retina: a reduction in density and the sprouting of dendrites. Although the thickness of the ONL did not change, it is very likely that the functions of the photoreceptors were compromised. The dramatic sprouting of rod bipolar cell dendrites is an indication of synaptic disfunction of the rod photoreceptor terminals. Since the rat retina is a rod dominating retina (Szél and Röhlich, 1992), loss of rod contacting bipolar cell dendrites alone could account for the loss of another major component of the OPL.

Alterations insensitive to treatment

In the OIR model, we noticed that the density of calretinin positive cells and the distance between innermost calretinin band and the border of RGC layer was reduced throughout the retina. Treatment of reducing IOP did not result in any remedy. These impairments may be the structural correlates of the residual impairments in visual functions. The calretinin labels at least two populations of amacrine cells, cholinergic amacrine cells in the INL and the GCL, and other

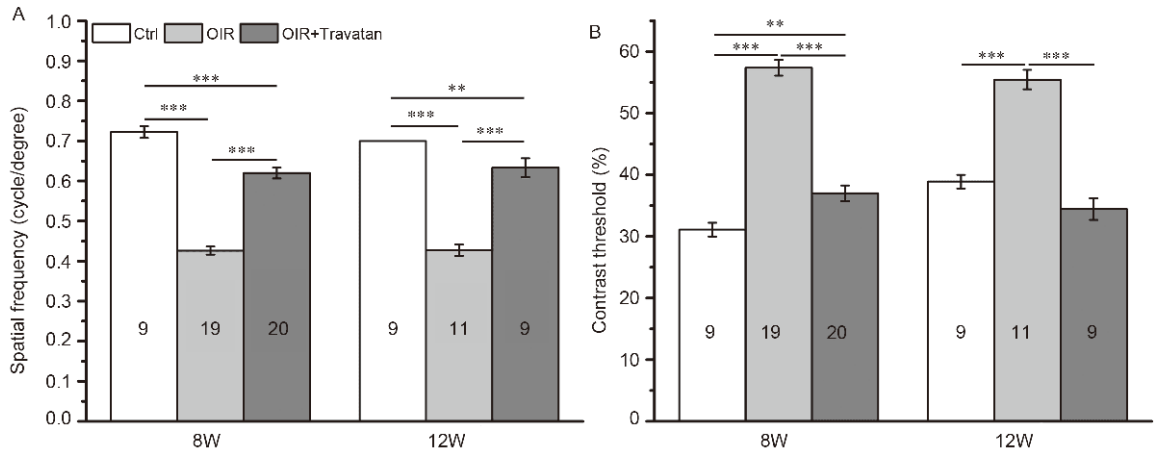

Figure 7 Visual acuity and contrast threshold measured by water visual task correct rate above 70%. The visual acuity of OIR group decreased from 0.72 ±0.01 (cpd) to 0.43±0.01 (cpd) and the OIR+Travatan group rescued to about 0.62±0.01 (cpd) at 8-week-old. At 12-week-old, the data were 0.7 (cpd), 0.43 ±0.01 (cpd) and 0.63±0.02 (cpd), respectively (A). The contrast threshold of OIR group increased from 31.11%±1.11% to 57.37%±1.29% and the treatment group rescued to 37.00%±1.23% at 8-week-old. The data were 38.89%±1.11%, 55.45%±1.58% and 34.44%±1.76%, respectively, at 12-week-old (B). **, $P<0.01$; ***, $P<0.001$.

amacrine cells stratifying in between the cholinergic bands. The decrease in density only took place in the INL. It is likely that the hypoxia only affected the amacrine cells other than cholinergic amacrine cells. The sublamina exhibiting significant reduction is the innermost ON sublamina of the IPL where the axon terminals of rod bipolar cells reside (Euler and Wässle, 1995; Ghosh et al., 2004). It is possible that the axon terminals of the rod bipolar cells would also be abnormal in addition to their dendrites. The incompatible factor is that the changes in dendrites and density of rod bipolar cells were only seen in the central retina, but the change of thickness of the IPL was both in the central and peripheral retina.

CONCLUSION

We reported in this study that reducing IOP in the rodent OIR model increased retinal vessel density, reverted most cytoarchitectral changes, and rescued visual function. More importantly, all these restorations persist for an extended period of time. Since the medicine is clinically administered, this approach could be a noninvasive, easily applicable and economically affordable therapy for ROP.

MATERIALS AND METHODS

Rat model of OIR

Pregnant Sprague-Dawley rats were used from experimental animal center of Shanghai Jiao Tong University (Shanghai, China). All procedures in this study were performed in accordance with the ARVO Statement for the Use of Animals in Ophthalmic and Vision Research and approved by guidelines of Institutional Animal Care and Use Committee (IACUC) of Shanghai Jiao Tong University. Rats were housed in a 12:12 h light-dark cycle and received food and water *ad libitum*. The number of retinas used in each experiment was indicated in the corresponding figure legend and table. The number of rats measured behavior visual function is shown in Figure 7. Each independent experiment included control (4), disease (4) and treatment (4) groups. When the number of pups was less than 12, we tried to maximize the number of animals in the disease and treatment groups.

The rat retina is immature at birth and corresponds to human fetus of 24–26 weeks (Ricci, 1990). The OIR model was performed as described (Wang et al., 2019). Briefly, neonatal rats and their nursing mother were exposed to 80% O_2 for 5 days (from P7 to 12). Oxygen concentration was monitored regularly with an oxygen analyzer (CY-12C, Shu Kang, China). Nursing mothers were alternated every day between two groups for exposure over 24 h to high oxygen could be fatal to adult rats. At P12, the animals were returned to room air.

Decreasing intraocular pressure

In the treatment group, 5 μL of Travatan (0.004% travoprost, Alcon, Spain) eye drop was applied to each eye from P12 to P19 twice daily (9 a.m. and 9 p.m.). 5 μL of 0.9% NaCl was applied to the eyes of OIR rats (no treatment) and control rats (no OIR, no treatment) as a control. We also reduced the IOP by puncturing the sclera physically to exclude side effects other than the decrease of IOP.

To measure the intraocular pressure, the rats were anesthetized by intraperitoneal injection of chloral hydrate (400 mg kg^{-1}, Sinopharm Chemical Reagent Co., Ltd, Chi-

na). Then 0.5% proparacaine hydrochloride (Alcon, Belgium) was applied topically to both eyes. IOPs were measured before and after eye drops treatment or sclera puncture using a rebound tonometer (TonoLab; Tiolat, Oy, Finland). The measurement was the averaged by the tonometer after six consecutive probe-to-cornea contacts.

Immunostaining on retinal sections and whole mount retina

Animals were deeply anesthetized with chloral hydrate (400 mg kg^{-1}) by intraperitoneal injection and intracadially perfused with phosphate buffer saline (0.1 mol L^{-1} PBS) followed by 4% paraformaldehyde (PFA, P6148; Sigma, USA) in 0.1 mol L^{-1} PBS. Eyes were enucleated and fixed in 4% PFA for 1 h at 4°C. After fixation, the cornea, lens and vitreous were carefully removed and retinas were dissected from the sclera. The fixed retinas were transferred to an ascending series of sucrose solution (10%, 20% and 30% in PBS) for cryoprotection. Then retinas were embedded in O. C.T Compound (Tissue-Tek, Sakura, USA) and 18 μm sections were cut by cryostat (CM1950, Leica, Germany).

The retinal sections were treated with a medium containing 1% BSA to block non-specific binding, 0.3% Triton X-100 to permeate cell membrane and 0.01% sodium azide in 0.1 mol L^{-1} PBS for 30 min. Then retina sections were incubated with primary antibodies in blocking buffer overnight at 4°C. After rinsing with PBS (3 times, 5 min each), sections were incubated with secondary antibody for 2 h at room temperature. DAPI (1:10,000, Sigma, USA) was added during the second incubation to stain the nucleus. The retinal sections were washed with PBS (3 times, 5 min each) and mounted in anti-fade mounting medium (H-1000, vector, USA). The primary and second antibodies used in this study are shown in Table 1. Images were captured using confocal microscopy (TCS SP8, Leica). Images were taken from 0–500 μm at both ends of the section considered as peripheral retina, and the remaining region of the section as the central retina. Each section was divided into 6 equal fields (2 fields of the peripheral retina and 4 fields of central retina). Within each field we measured the average thickness of sublaminae, density of soma and length of dendrites with ImageJ (NIH, Bethesda, MD) and adjusted for brightness and contrast with photoshop CS6 (Adobe System, USA). The average of 4 sections was the measurement for each sample.

To stain whole mount retina, the retinas were incubated with buffer A for 5 days at 4°C to permeate the membrane and block non-specific binding sites. The retinas were washed in PBS 3 times for 15 min. Then the retinas were incubated with Griffonia simplicifolia Isolection GS-IB4 conjugated to Alexa Fluor 488 (1:100, I21411, Invirogen, USA) for 48 h at 4°C. After rinsing with PBS, the retinas were mounted in an anti-fade mounting medium. For quantification of vessel density, images were taken from an optic disc to the peripheral retina in four quadrants as described (Wang et al., 2019). In brief, 6 images were taken in each axis from the optic disc to far periphery using a confocal microscope (TCS SP8, Leica). The threshold of each image was calculated to differentiate vessels from background using IsoData method by ImageJ (Schneider et al., 2012). The vessel density was the percentage of pixels above the threshold. The average vessel density of all images (24 images) from a retina was taken as the vessel density of the retina. The vessel density in the superficial and deep layer was calculated separately.

Behavioral test of visual function

The apparatus and methods used to measure rat visual behavior including both visual acuity and contrast sensitivity in this study have been described previously (Prusky et al., 2000; McGill et al., 2004; Ren et al., 2012; Zhou et al., 2017; Wang et al., 2019). Briefly, a trapezoidal-shaped pool with two computer monitors facing to the wider side of the pool. Visual stimuli (square-wave grating and uniform luminance) were controlled by Visual Studio 2014 (Microsoft, USA) and played on the monitors. A transparent platform (37 cm long× 13 cm wide×14 cm high) was hidden under the surface of the water directly below the monitor displaying the grating. The location of the grating was pseudorandom.

There were three phases to the task: pre-training conditioning, task training and contrast and acuity test. All trials were run with dark environment. In pre-training phase, animals were conditioned gradually to locate a platform hidden below a screen. In the training phase, rats were conditioned

Table 1 List of the antibodies and sources using in this study

Antigen	Species	Cellular specificity	Dilution	Supplier
PKCα	Rabbit polyclonal	Bipolar cell	1:10,000	Sigma
Calbindin	Mouse monoclonal	Horizontal cell	1:100	Sigma
Calretinin	Rabbit polyclonal	Amacrine cell	1:2,000	Millipore
Rabbit	Donkey	IgG (H+L) Alexa Fluor® 647-conjugated	1:200	Jackson Immunoresearch
Mouse	Goat	IgG (H+L) FITC conjugated	1:200	Jackson Immunoresearch
Rabbit	Goat	IgG (H+L) FITC conjugated	1:200	Jackson Immunoresearch

to swim from a release chute and to associate the platform with the screen displaying gratings using low spatial frequency (0.1 cycles/degree, 0.1 cpd) and high contrast (100%) gratings. Rats were trained 10 trials per session, and less than three sessions, separated by at least 1 h, were performed in a single day. Once animals achieved above 80% correct rate in successive 30 trials, the acuity and contrast were then measured. In the contrast sensitivity test, each rat performed 10 trials for each contrast (decrement step 10%) and its correct rate was recorded. In the visual acuity test, each animal performed 10 trials for each spatial frequency grating (increment step 0.1 cpd) and the correct rate recorded. When the correct rate fell below 70%, the spatial frequency test or contrast sensitivity test was terminated and measurements taken as the detection threshold.

Statistical analysis

All results were presented as mean±SEM. Statistical analysis was performed using one-way ANOVA followed by Newman-Keuls Test for multiple comparisons (OriginPro 2016, OriginLab, USA). $P<0.05$ were considered statistically significant.

Compliance and ethics *The author(s) declare that they have no conflict of interest. All authors certify that they have no affiliations with or involvement in any organization or entity with any financial interest, or non-financial interest in the subject matter or materials discussed in this manuscript. All procedures performed in studies involving animals were in accordance with the ethical standards of the institution or practice at which the studies were conducted.*

Acknowledgements *We thank Ms. Jiaying Ju for technical support. This work was funded by a key project of the National Natural Science Foundation of China (31030036) to SH.*

References

Asano, M.K., and Dray, P.B. (2014). Retinopathy of prematurity. Dis Mon 60, 282–291.
Ashton, N. (1954). Pathological basis of retrolental fibroplasia. Br J Ophthalmol 38, 385–396.
Ashton, N., Ward, B., Serpell, G. (1953). Role of oxygen in the genesis of retrolental fibroplasia. ; Ashton, N., Ward, B., and Serpell, G. (((1953))). Role of oxygen in the genesis of retrolental fibroplasia: a preliminary report. Br J Ophthalmol 37, 513–520.
Campbell, K. (1951). Intensive oxygen therapy as a possible cause of retrolental fibroplasia; a clinical approach. Med J Aust 2, 48.
Chung, E.J., Kim, J.H., Ahn, H.S., and Koh, H.J. (2007). Combination of laser photocoagulation and intravitreal bevacizumab (Avastin®) for aggressive zone I retinopathy of prematurity. Graefes Arch Clin Exp Ophthalmol 245, 1727–1730.
Connor, K.M., Krah, N.M., Dennison, R.J., Aderman, C.M., Chen, J., Guerin, K.I., Sapieha, P., Stahl, A., Willett, K.L., and Smith, L.E.H. (2009). Quantification of oxygen-induced retinopathy in the mouse: a model of vessel loss, vessel regrowth and pathological angiogenesis. Nat Protoc 4, 1565–1573.
Early Treatment for Retinopathy of Prematurity Cooperative Group. (2003). Revised indications for the treatment of retinopathy of prematurity: results of the early treatment for retinopathy of prematurity randomized trial. Arch Ophthalmol (Chicago, Ill: 1960) 121, 1684.
Elsas, F., Botsford, J., Braune, K., Cassady, G., Jones, J., Kimble, J., Kline, L., Lampton, G., Witherspoon, D., and Young, M. (1988). Multicenter trial of cryotherapy for retinopathy of prematurity: preliminary results. Pediatrics 81, 697–706.
Elsas, F, Collins, M, Jones, J, Kimble, J, Kline, L, Witherspoon, D, Roth, A, Demorest, B, Gilbert, W, and Plotsky, D (2001). Multicenter trial of cryotherapy for retinopathy of prematurity. Arch Ophthalmol 119, 1110–1118.
Euler, T., and Wässle, H. (1995). Immunocytochemical identification of cone bipolar cells in the rat retina. J Comp Neurol 361, 461–478.
Friedenwald, J.S., Owens, W.C., and Owens, E.U. (1951). Retrolental fibroplasia in premature infants. III. The pathology of the disease. Trans Am Soc Ophthalmol Otolaryngol Allergy 49, 207–234.
Ghosh, K.K., Bujan, S., Haverkamp, S., Feigenspan, A., and Wässle, H. (2004). Types of bipolar cells in the mouse retina. J Comp Neurol 469, 70–82.
Goldenberg, R.L., Culhane, J.F., Iams, J.D., and Romero, R. (2008). Epidemiology and causes of preterm birth. Lancet 371, 75–84.
Kolb, H. (1974). The connections between horizontal cells and photoreceptors in the retina of the cat: electron microscopy of Golgi preparations. J Comp Neurol 155, 1–14.
Krause, A.C. (1946). Congenital encephalo-ophthalmic dysplasia. Arch Ophthalmol 36, 387–444.
Lange, C., Ehlken, C., Stahl, A., Martin, G., Hansen, L., and Agostini, H.T. (2009). Kinetics of retinal vaso-obliteration and neovascularisation in the oxygen-induced retinopathy (OIR) mouse model. Graefes Arch Clin Exp Ophthalmol 247, 1205–1211.
Liu, L., Li, X., Killer, H.E., Cao, K., Li, J., and Wang, N. (2019). Changes in retinal and choroidal morphology after cerebrospinal fluid pressure reduction: a Beijing iCOP study. Sci China Life Sci 62, 268–271.
Lorenz, B., Spasovska, K., Elflein, H., and Schneider, N. (2009). Wide-field digital imaging based telemedicine for screening for acute retinopathy of prematurity (ROP). Six-year results of a multicentre field study. Graefes Arch Clin Exp Ophthalmol 247, 1251–1262.
McGill, T.J., Douglas, R.M., Lund, R.D., and Prusky, G.T. (2004). Quantification of spatial vision in the Royal College of Surgeons rat. Invest Ophthalmol Vis Sci 45, 932–936.
McNamara, J.A., Tasman, W., Brown, G.C., and Federman, J.L. (1991). Laser photocoagulation for stage 3+ retinopathy of prematurity. Ophthalmology 98, 576–580.
Mintz-Hittner, H.A., Kennedy, K.A., Chuang, A.Z., and Chuang, A.Z. (2011). Efficacy of intravitreal bevacizumab for stage 3+ retinopathy of prematurity. N Engl J Med 364, 603–615.
Moskowitz, A., Hansen, R., and Fulton, A. (2005). Early ametropia and rod photoreceptor function in retinopathy of prematurity. Optom Vis Sci 82, 307–317.
O'Connor, A.R., Stephenson, T.J., Johnson, A., Tobin, M.J., Ratib, S., Moseley, M., and Fielder, A.R. (2004). Visual function in low birthweight children. Br J Ophthalmol 88, 1149–1153.
Patz, A. (1954). Oxygen studies in retrolental fibroplasia. IV. Clinical and experimental observations. Am J Ophthalmol 38, 291–308.
Patz, A. (1982). Clinical and experimental studies on retinal neovascularization. Am J Ophthalmol 94, 715–743.
Patz, A., Eastham, A., Higginbotham, D.H., and Kleh, T. (1953). Oxygen studies in retrolental fibroplasia. II. The production of the microscopic changes of retrolental fibroplasia in experimental animals. Am J Ophthalmol 36, 1511–1522.
Patz, A., Hoeck, L.E., and De La Cruz, E. (1952). Studies on the effect of high oxygen administration in retrolental fibroplasia. I. Nursery observations. Am J Ophthalmol 35, 1248–1253.
Peichl, L., and Gonzalez-Soriano, J. (1993). Unexpected presence of neurofilaments in axon-bearing horizontal cells of the mammalian retina. J Neurosci 13, 4091–4100.
Penn, J.S., Tolman, B.L., and Lowery, L.A. (1993). Variable oxygen exposure causes preretinal neovascularization in the newborn rat. Invest

Ophthalmol Vis Sci 34, 576–585.
Prusky, G.T., West, P.W.R., and Douglas, R.M. (2000). Behavioral assessment of visual acuity in mice and rats. Vis Res 40, 2201–2209.
Qiao, L., Zhang, X., Jan, C., Li, X., Li, M., and Wang, H. (2019). Macular retinal thickness and flow density change by optical coherence tomography angiography after posterior scleral reinforcement. Sci China Life Sci 62, 930–936.
Ren, R., Li, Y., Liu, Z., Liu, K., and He, S. (2012). Long-term rescue of rat retinal ganglion cells and visual function by AAV-mediated BDNF expression after acute elevation of intraocular pressure. Invest Ophthalmol Vis Sci 53, 1003–1011.
Ricci, B. (1990). Oxygen-induced retinopathy in the rat model. Doc Ophthalmol 74, 171–177.
Ricci, B., Calogero, G., Caprilli, A., and Quaranta-Leoni, F.M. (1991). Reduced severity of oxygen-induced retinopathy in the newborn rat after topical administration of timolol maleate. Doc Ophthalmol 77, 47–56.
Sandman, D., Boycott, B.B., and Peichl, L. (1996). The horizontal cells of artiodactyl retinae: a comparison with Cajal's descriptions. Vis Neurosci 13, 735–746.
Schneider, C.A., Rasband, W.S., and Eliceiri, K.W. (2012). NIH Image to ImageJ: 25 years of image analysis. Nat Methods 9, 671–675.
Shah, P.K., Narendran, V., Tawansy, K.A., Raghuram, A., and Narendran, K. (2007). Intravitreal bevacizumab (Avastin) for post laser anterior segment ischemia in aggressive posterior retinopathy of prematurity. Ind J Ophthalmol 55, 75–76.
Smith, L.E.H. (2003). Pathogenesis of retinopathy of prematurity. Semin Neonatol 8, 469–473.
Smith, L.E., Wesolowski, E., Mclellan, A., Kostyk, S.K., D'amato, R., Sullivan, R., and D'amore, P.A. (1994). Oxygen-induced retinopathy in the mouse. Invest Ophthalmol Vis Sci 35, 101–111.
Stahl, A., Krohne, T.U., Eter, N., Oberacher-Velten, I., Guthoff, R., Meltendorf, S., Ehrt, O., Aisenbrey, S., Roider, J., Gerding, H., et al. (2018). Comparing alternative ranibizumab dosages for safety and efficacy in retinopathy of prematurity. JAMA Pediatr 172, 278–286.
Suzuki, H., and Pinto, L. (1986). Response properties of horizontal cells in the isolated retina of wild- type and pearl mutant mice. J Neurosci 6, 1122–1128.
Szél, Á., and Röhlich, P. (1992). Two cone types of rat retina detected by anti-visual pigment antibodies. Exp Eye Res 55, 47–52.
Wang, X., Shen, K., Lu, F., and He, S. (2019). Long-lasting impairments in rodent oxygen-induced retinopathy measured by retinal vessel density and visual function. Sci China Life Sci 62, 681–690.
Xin, C., Tian, N., Li, M., Wang, H., and Wang, N. (2018). Mechanism of the reconstruction of aqueous outflow drainage. Sci China Life Sci 61, 534–540.
Zhang, J., Jia, H., Wang, J., Xiong, Y., Li, J., Li, X., Zhao, J., Zhang, X., You, Q., Zhu, G., et al. (2019). A novel deletion mutation, c.1296delT in the BCOR gene, is associated with oculo-facio-cardio-dental syndrome. Sci China Life Sci 62, 119–125.
Zhang, X., Yuan, Q., and Gao, X. (2018). Assessment of the MT1-MMP expression level of different cell lines by the naked eye. Sci China Life Sci 61, 492–500.
Zhou, Y., Xiao, C., and Pu, M. (2017). High glucose levels impact visual response properties of retinal ganglion cells in C57 mice—An *in vitro* physiological study. Sci China Life Sci 60, 1428–1435.

SUPPORTING INFORMATION

Figure S1 IOP measurement after administering Travatan eye drops of puncturing the sclera.

Figure S2 The measurement of immeasurable OPL length of OIR and OIR+Travatan group at 8-week-old and 12-week-old.

Figure S3 The tendency of visual acuity and contrast threshold.

The supporting information is available online at http://life.scichina.com and https://link.springer.com. The supporting materials are published as submitted, without typesetting or editing. The responsibility for scientific accuracy and content remains entirely with the authors.